ADVANCED FUNCTIONAL MATERIALS
www.afm-journal.de

Ballistic Ejection of Microdroplets from Overpacked Interfacial Assemblies

Xuefei Wu, Gautam Bordia, Robert Streubel, Jaffar Hasnain, Cássio C.S. Pedroso, Bruce E. Cohen, Behzad Rad, Paul Ashby, Ahmad K. Omar, Phillip L. Geissler, Dong Wang,* Han Xue, Jianjun Wang, and Thomas P. Russell**

Dedicated to the memory of Phillip L. Geissler, an exceptional colleague, scientist, and collaborator, without whom this work would not have been possible

Spontaneous emulsification, resulting from the assembly and accumulation of surfactants at liquid–liquid interfaces, is an interfacial instability where microdroplets are generated and diffusively spread from the interface until complete emulsification. Here, it is shown that an external magnetic field can modulate the assembly of paramagnetic nanoparticle surfactants (NPSs) at liquid–liquid interfaces to trigger an oversaturation in the areal density of the NPSs at the interface, as evidenced by a marked reduction in the interfacial tension, γ, and corroborated with a magnetostatic continuum theory. Despite the significant reduction in γ, the presence of the magnetic field does not cause stable interfaces to become unstable. Upon rapid removal of the field, however, an explosive ejection of a plume of microdroplets from the surface occurs, a dynamical interfacial instability which is termed explosive emulsification. This explosive event rapidly reduces the areal density of the NPSs to its pre-field level, stabilizing the interface. The ability to externally suppress or trigger the explosive emulsification and controlled generation of tens of thousands of microdroplets, uncovers an efficient energy storage and release process, that has potential applications for controlled and directed delivery of chemicals and remotely controlled soft microrobots, taking advantage of the ferromagnetic nature of the microdroplets.

1. Introduction

The use of paramagnetic nanoparticle surfactants (NPSs) provides additional control of surfactant adsorption through the application of an external magnetic field (in addition to the more canonical control variables of surfactant concentration and solution chemistry, e.g., pH).[1] Magnetic field gradients are widely used to steer the movement of objects or to realize function, including rotation, swimming, rolling, and transport of cargo.[2] A magnetic field also induces a magnetic dipole moment in superparamagnetic particles. When the interparticle dipole interaction energy is large enough to overcome thermal energy, the dipolar force drives the assembly of magnetic particles into chain-like structures at low particle concentrations,[3] where the interparticle distance can be finely tuned by balancing the

X. Wu, D. Wang, T. P. Russell
Beijing Advanced Innovation Center for Soft Matter Science and Engineering & State Key Laboratory of Organic-Inorganic Composites
Beijing University of Chemical Technology
Beijing 100029, China
E-mail: dwang@mail.buct.edu.cn; russell@mail.pse.umass.edu

X. Wu, G. Bordia, J. Hasnain, A. K. Omar, T. P. Russell
Materials Sciences Division
Lawrence Berkeley National Laboratory
Berkeley, CA 94720, USA
E-mail: aomar@berkeley.edu

G. Bordia, A. K. Omar
Department of Materials Science and Engineering
University of California
Berkeley, CA 94720, USA

R. Streubel
Department of Physics and Astronomy
University of Nebraska-Lincoln
Lincoln, NE 68588, USA

The ORCID identification number(s) for the author(s) of this article can be found under https://doi.org/10.1002/adfm.202213844.

DOI: 10.1002/adfm.202213844

J. Hasnain, P. L. Geissler
Department of Chemistry
University of California
Berkeley, CA 94720, USA

C. C.S. Pedroso, B. E. Cohen, B. Rad, P. Ashby
Molecular Foundry
Lawrence Berkeley National Laboratory
Berkeley, CA 94720, USA

B. E. Cohen
Division of Molecular Biophysics & Integrated Bioimaging
Lawrence Berkeley National Laboratory
Berkeley, CA 94720, USA

H. Xue, J. Wang
Beijing National Laboratory for Molecular Science
Institute of Chemistry
Chinese Academy of Sciences
Beijing 100190, China

T. P. Russell
Polymer Science and Engineering Department
University of Massachusetts
Amherst, MA 01003, USA

T. P. Russell
Advanced Institute for Materials Research (AIMR)
Tohoku University
2-1-1 Katahira, Aoba, Sendai 980–8577, Japan

magnetic field strength against interparticle repulsion.[4] With increasing particle concentration, multiple chains can aggregate into zigzag assemblies, 2D labyrinths, and 3D structures. Here, we found that the magnetic field can be used to drive the interface of a droplet into a highly unstable state by oversaturating the interface with paramagnetic nanoparticle surfactants such that, upon a rapid release of the field, an explosive emulsification occurs, where the unstable liquid–liquid interface rapidly generates additional surface area by the formation and ejection of tens of thousands of microdroplets from the interface at high velocities.[5]

Various mechanisms of spontaneous emulsification have been proposed. Some are mechanical, including interfacial turbulence and interfacial expansion due to a negative interfacial tension,[6] others are based on phase transformations with the formation of localized areas of supersaturation of surfactants/cosolvents at the interface.[7] Still other origins have been proposed, including a) osmotic pressure gradients,[8] b) hydrogen bonding between the surfactants and water increasing the solubility of water in the oil phase;[9] and c) changes in temperature, pH, or concentration.[5d,10] Here, we report a fundamentally different form of emulsification that is triggered by a high interfacial stress resulting from an oversaturation of the NPSs at the interface by use of an external magnetic field. Due to their strong interfacial activity, if the adsorption of NPSs to a fluid interface reduces the interfacial tension to a low enough value, traditional spontaneous emulsification is observed with the formation of NPS-covered microdroplets that diffuse away from the interface.[5a] When the interface is stable, absent an applied field, no instability is observed when a field is applied, even though the interface is oversaturated with NPSs. However, rapidly removing the external field results in an explosive event in which ferromagnetic microdroplets are ballistically ejected from the interface at large ejection velocities. Following this initial explosive emulsification, ferromagnetic microdroplets continue to be released from the parent droplet until the equilibrium NPS surface coverage is restored. Rather than requiring a chemical reaction or meeting specific physiochemical conditions, this unique interfacial response may provide new strategies for the design of micro-ferromagnetic liquid droplet systems and remotely controlled soft microrobots.[1e,11] More fundamentally, the use of a magnetic field allows a precise temporal control of the interfacial assembly, enabling a systematic interrogation of interfacial instabilities.

2. Results and Discussion

2.1. pH Dependence of NPSs Assembly

Carboxylated 30 nm diameter paramagnetic nanoparticles (Fe_3O_4-CO_2H) dispersed in an aqueous medium do not assemble at an interface with an apolar solvent, like toluene.[12] However, with the addition of the triamine-modified polystyrene (PS-triNH_2), a cationic surfactant, to the oil phase, the protonated PS-triNH_3^+ is able to electrostatically interact with and anchor to the negatively charged Fe_3O_4 NPs to form paramagnetic NPSs at the interface, markedly increasing the binding energy of the nanoparticles to the interface.[1f-h,13] We note that the charge density and binding energy of NPSs are pH-dependent. Under acidic conditions, the amine groups tend to be protonated and the PS-triNH_3^+ exhibits high interfacial activity, which attracts abundant negatively charged NPs to the interface and leads to the formation of NPSs that have a high binding energy and are in a weakly charged state. This could result in a dense packing and even jamming of the NPSs at the interface.[1f,g] However, in neutral or alkaline conditions, with fewer amine groups protonated at the interface, less NPSs are formed, and, due to the deprotonation of the carboxyl groups on the NPs' surfaces, there are strong electrostatic repulsions between the NPSs, decreasing the interfacial coverage as evidenced by a higher interfacial tension (Figure S2, Supporting Information).

2.2. Magnetic Field Induced Oversaturation

An external magnetic field induces a magnetic moment in a paramagnetic particle $m = \chi HV$, where χ is the volume susceptibility of the particle (Fe_3O_4), H is the applied magnetic field strength, and V the volume of the particle. When dipolar interactions are strong enough to overcome thermal fluctuations and balance electrostatic repulsions between the particles, the magnetic dipolar force densifies the assembly in a direction along the dipole moment,[3c,4,14] where the interparticle distance can be tuned with the strength of the magnetic field.[4] A monotonic reduction in the effective interfacial tension is observed with increasing field strength, as shown in **Figure 1**a. The effective interfacial tension is the difference between the bare or intrinsic surface tension between the two liquids, $\gamma_{o/w}$, and the in-plane pressure, P_{2D}, exerted by the NPSs (i.e., $\gamma = \gamma_{o/w} - P_{2D}$). The significant increase in the in-plane pressure exerted by nanoparticles with the applied field provides compelling indirect evidence for the increased adsorption of NPSs induced by the applied field. The binding energy of the nanoparticles to the interface is governed by the interfacial energy between the liquids and NPSs material properties that are not altered by the magnetic field.

At neutral/alkaline conditions, where the interfacial packing is dominated by electrostatic repulsions, the application of the external magnetic field can balance the electrostatic repulsion,

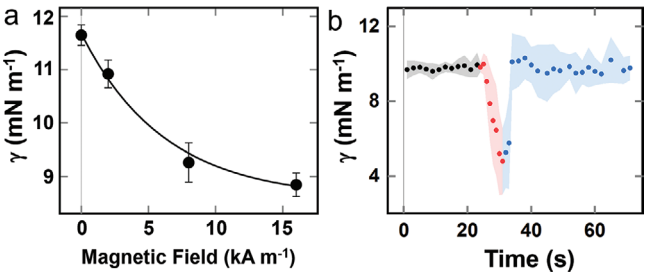

Figure 1. Magnetic field dependence of interfacial tension, γ. a) Relationship between the equilibrium γ value and the applied magnetic field. b) Temporal evolution of γ between the aqueous and toluene phase before (black dots with error band), during (red dots with error band), and after (blue dots with error band) the magnetization of nanoparticle surfactants by an external magnetic field (≈175 kA m^{-1}). The concentrations of Fe_3O_4-CO_2H and PS-triNH_2 are 1 mg mL^{-1}; pH of aqueous phase is 7.

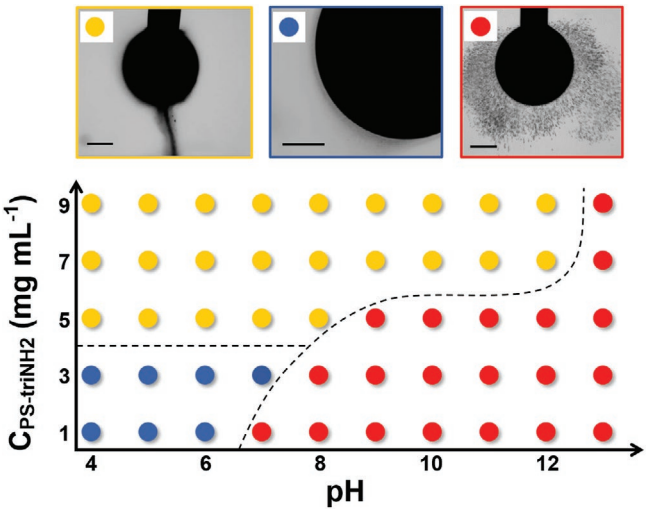

Figure 2. Interfacial stability diagram. Surfactant concentration ($C_{PS\text{-}triNH2}$) and pH dependencies of spontaneous and explosive emulsification in the strong magnetic field limit (175 kA m^{-1}). Spontaneous emulsification (filled gold circle and filled blue circle) is identified through the constant ejection of microdroplets at lower pH and high surfactant concentration. Explosive emulsification (filled red circle) occurs only upon rapid removal of the field (the field retraction rates up to tens of mm s^{-1}). The dashed line serves as a guide-to-the-eye. Scale bar for the image insets is 500 µm.

densify the assembly, and "quench" it into an oversaturated state. In bulk dispersions, this process is usually reversible, and with the field removed, electrostatic repulsion drives the particles away from each other.[3b,15] For the interfacial assemblies, though, the binding energy per particle competes with the potential energy after the field is removed. The binding energy of the NPSs, formed by the attachment of multiple hydrophobic ligands to the polar NP, is greatly increased, which inhibits the desorption of the NPs from the interface.[1f] As a result, the oversaturated packing of the NPSs is able to raise the in-plane pressure after the field is turned off, triggering the explosive emulsification (Video S1, Supporting Information) and rapidly increasing the interfacial tension of the parent drop to its equilibrium value (Figure 1b). The ejection velocities decrease with increasing pH (**Figure 2** (filled red circles); Figure S3, Supporting Information).

At low pH and high surfactant concentration, most amine groups are protonated and strongly anchor the surfactants to the Fe_3O_4-CO_2H. These conditions result in high NPS surface coverage, as indicated by a significantly reduced γ (Figure S2, Supporting Information) and can ultimately result in spontaneous emulsification where a steady stream of microdroplets flows from the base of the parent droplet (Figure 2 (filled gold circles); Video S2, Supporting Information).[5a] For systems undergoing spontaneous emulsification prior to the application of a field (i.e., low pH and high surfactant concentration), emulsification continues and appears slightly suppressed by the presence of the field (Figure S4, Supporting Information). Spontaneous emulsification can also produce a diffuse ring of micro droplets several tens of micrometers away from the parent drop surface (Figure S5, Supporting Information) at lower ligand concentrations and pH (Figure 2 (filled blue circles)), indicative of an electrostatic repulsion between the parent droplet and the microdroplets. (Figure S3, Supporting Information)

2.3. Mechanisms of Explosive Emulsification

We leverage computer simulations and continuum theory to reveal the nature of the field-induced driving force for the migration of NPSs to the interface. A representative equilibrium configuration of dipolar magnetic particles confined to the surface of a sphere (representing the parent droplet) in the presence of a uniform magnetic field is obtained from computer simulations (see Supporting Information) and depicted in **Figure 3**a. The polarization magnitude of nanoparticles is spatially inhomogeneous along the droplet's surface, with a greater degree of polarization along the field direction near the droplet equator. The magnetic field generated by the interfacial dipolar particles is shown in Figure 3b and reveals significant and nearly uniform magnetic screening of the droplet interior. This screening effect, together with the enhanced polarizability of a particle within the dense shell comprising the interfacial assembly, results in a significant driving force for particle migration to the interface. As shown in Figure 3c, the chemical potential within the droplet shell (representing the interface) is lower than in the droplet interior. In the framework of linear irreversible thermodynamics, chemical potential gradients drive particle migration.[16] The lower magnetic chemical potential would thus drive particle migration from the droplet interior to the interface until the total chemical potential (which includes contributions from translational entropy and non-magnetic inter-nanoparticle interactions, discussed in our previous work)

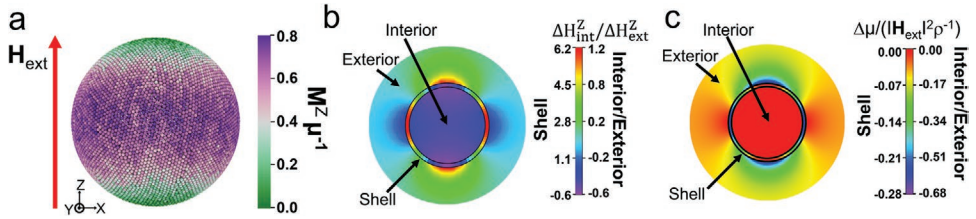

Figure 3. Thermodynamics of interfacial magnetic dipolar particles. a) Instantaneous simulation configuration of dipolar magnetic particles bound to a spherical surface (50 times larger in diameter than the particles with a surface areal fraction of $\eta = 0.8$) in the presence of a uniform magnetic field. The magnetic field strength is kept weak to facilitate a comparison with linear response theory. b) Spatial distribution of the interfacial particle induced field computed in simulations (see Supporting Information for details) reveals a spatially inhomogeneous magnetic environment, in agreement with linear response theory (Supporting Information). c) Linear response prediction for the spatial distribution of the magnetic contribution to the nanoparticle chemical potential. Here we take a magnetic permeability $\varepsilon = 50$ and shell thickness to droplet diameter ratio to be 1:50. Results for thinner shells and other permeabilities give qualitatively similar results.

is spatially uniform.[5a] Linear response theory confirms these findings (see Supporting Information) and allows us to provide a more direct measure of the driving force for interfacial particle migration through the magnetic chemical potential (Figure 3c).

Despite the enhanced NPS surface coverage resulting in what can be up to an order of magnitude decrease in the γ from the pre-field value, the aqueous droplets remain stable while the field is present. For systems that were stable but near the emulsification boundary in the absence of the field, one might expect that the field-induced increase in interfacial NPS coverage would provide the requisite driving force for emulsification. Nevertheless, emulsification was not observed despite the observed reduction of γ and the proximity to the emulsification boundary.

The apparent stability of these interfaces has several possible origins. One is that the interface, despite its high NPS coverage, is fully equilibrated and thus truly stable. The stability criteria for an interface are sensitive to the in-plane interactions between interfacial NPSs (or more directly the in-plane pressure, P_{2D}, exerted by the NPSs).[5a] The magnetic field acts to polarize the magnetic dipoles in the field-direction, which in turn alters the nanoparticle microstructure. While this undoubtedly affects the in-plane pressure tensor that is decreased under the magnetic field owing to the existence of dipolar–dipolar interaction based upon the Frumkin equation,[17] the degree to which this occurs is presently unclear. An alternative and intriguing possibility is that the droplet is metastable due to the NPS microstructure introducing a barrier to emulsification, the globally stable system configuration. As a well-established example of such metastability, liquid–liquid interfaces that are maximally packed or "jammed" with NPSs can persist indefinitely and exhibit solid-like properties.[1e–g,13b] A hallmark of these structured liquids is the development of an elastic response to interfacial deformation. In the present case of magnetic NPSs, however, the surface coverage is below the threshold for jamming as determined from wrinkling experiments (Figure S6, Supporting Information), where a wrinkle pattern is not observed on the pendant droplet surface during a reduction of the droplet volume.[1g]

2.4. Magnet Retraction Rate Dependence

Under conditions where the interface is stable in the absence of a field, application and removal of the magnetic field can lead to different scenarios depending on the field retraction rate. Removing the field introduces a thermodynamic driving force for the desorption of the excess NPSs back into the aqueous parent droplet until the equilibrium coverage is restored. As a result, removing the field quasi-statically (i.e., reversibly removing the external field) should result in the steady desorption of NPS into the aqueous phase and a return to stable interface.

If the field is instead removed at a finite rate, nonequilibrium dynamical effects may dominate the response. Since the degree of paramagnetic NPS adsorption increases with the magnetic field strength, we focus on strong magnetic field strengths (≈175 kA m^{-1}) with a magnetization time of ≈10 s before retracting the field (Figure S3e, Supporting Information) (see Experimental Section). Rapidly removing the external magnetic field allows for probing the irreversible limit and observing a forceful ejection of microdroplets after a short delay, that is, within 2 s after removal of the field (Figures S3 and S7, Supporting Information).

At the fastest removal rate, tens of thousands of microdroplets (**Figure 4**a), ≈4 μm in diameter, are ejected at a velocity of ≈3.7 mm s^{-1} (Figure 4b) and continue their persistent motion over 1–2 mm away from the parent droplet surface. This explosive event stabilizes the interface, reflected in the restoration of γ to its pre-field values 3 s after removing the field (Figure 1b). Decreasing the field removal rate monotonically reduces the number of ejected microdroplets and their ejection velocities, and, also, increases the delay time between field removal and the explosive event (Figure 4). The energy released through explosive emulsification is decreased at slower removal rate, where the remainder of the excess energy is dissipated by particle rearrangement and desorption from the interface. The diminishment of this explosive event with decreasing field removal rate is consistent with our expectation of no explosive behavior in the quasi-static limit.

While the ejection velocities of these microdroplets can be extraordinarily high, the colloidal scale of these droplets and the viscosity of the oil would suggest that low-Reynolds number physics is at play and inertial effects are negligible. The persistent motion for these large length scales is therefore likely the result of a persistent force acting on the microdroplets. Magnetic dipolar forces between the parent and microdroplets could provide an initial ejective force, but the ejected microdroplets would rapidly reorient to alleviate such a repulsion. The long-range nature of the force apparently propelling the microdroplets is highly suggestive of an electrostatic origin, which may be the result of overcharging the interface upon field removal. The magnetic field brings excess negatively charged Fe_3O_4 NP to the interface, which, we hypothesize, is similar to overcharging the interface with negative charges. When the field is on, the dipolar–dipolar interaction between the particles can stabilize the droplet in the overcharged state, which can return to equilibrium state by propelling the excess nanoparticles from the interface by explosive emulsification. Imaging experiments using upconverting nanoparticles,[18] whose emission is sensitive to sub-degree temperature changes,[19] did not show measurable temperature changes during the explosive emulsification, arguing against a latent heat origin of the observed behavior.

2.5. Characterization of the Microdroplets

The microdroplets produced during explosive emulsification and also spontaneous emulsification have a remnant magnetization. The remnant magnetization of microdroplets with an average diameter of ≈4 μm is found to be ≈1.7×10^{-16} A.m^2 and is calculated using the methods mentioned in Ref. [13c], and a sizable coercive field (ferromagnetism) as verified by their rotation in the presence of an external rotating magnetic field (**Figure 5**b; Video S3, Supporting Information).[13c,20] Previously, the development of ferromagnetism was associated with the

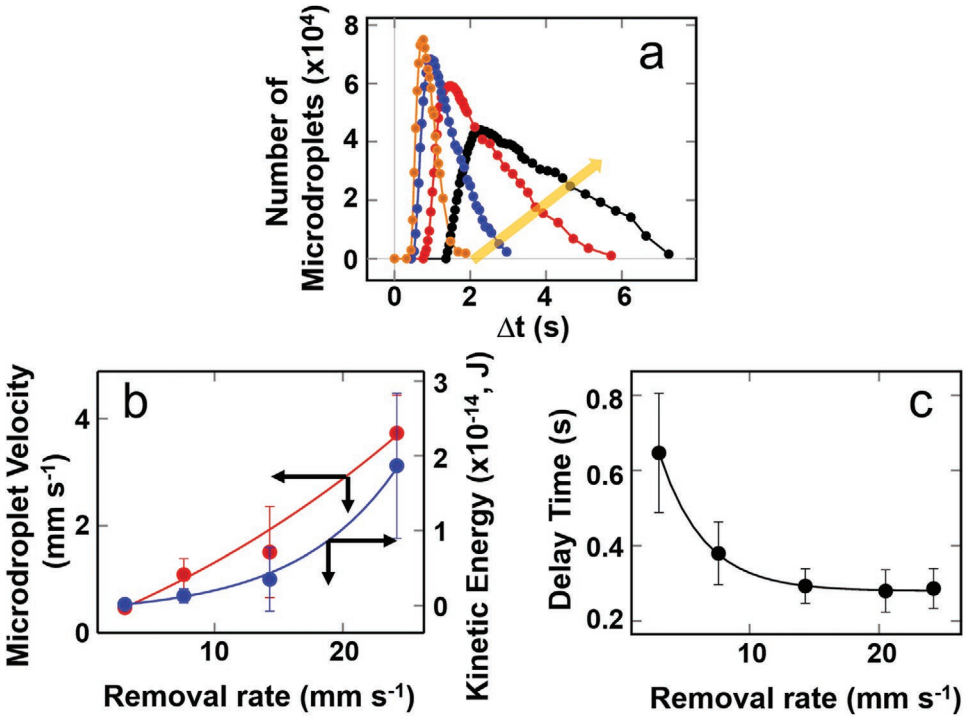

Figure 4. Influence of magnet retraction rate on explosive emulsification. a) Temporal evolution of the number of microdroplets produced after withdrawal of the bar magnet at various rates, 3.0 (black), 7.6 (red), 14.6 (blue), and 24.2 mm s^{-1} (orange). b) Initial velocity and total kinetic energy as a function of retraction velocity of bar magnet and, c) delay time for onset of explosive emulsification. The concentrations of Fe_3O_4-CO_2H and PS-triNH_2 are 1 mg mL^{-1}; pH of aqueous phase is 7.

jamming of paramagnetic NPSs at the interface.[1e,13c] This raises the intriguing possibility that despite the parent droplets being decidedly below the jamming transition, the microdroplets generated during explosive emulsification may have a NPS surface coverage that exceeds that of the parent droplet. In the long-time limit and in the absence of a field, these droplets should eventually merge with the parent droplet. The stability as evidenced by the long lifetime of the microdroplets, along with their ferromagnetism, supports the conclusion that they are in fact jammed (Figure 5b,c).

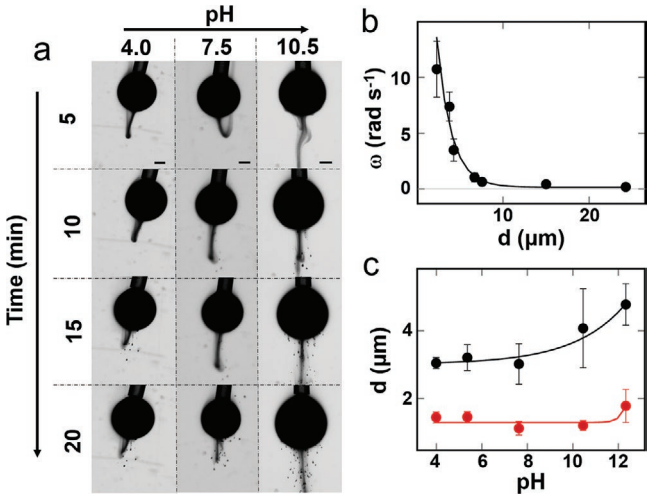

Figure 5. Spontaneous emulsification of aqueous droplets at high surfactant concentration. a) Snapshots of an aqueous droplet with different pH in the oil phase. Scale bar is 500 μm. b) Effect of microdroplet size, d, on the angular frequency, ω. The driving angular frequency is 80 rpm. c) Average diameter of the microdroplets as a function of pH. The black and red curves refer to fresh and 35-day old, respectively. The concentrations of Fe_3O_4-CO_2H and PS-triNH_2 are 1 and 7 mg mL^{-1}, respectively. The pH of the aqueous phase is 7.

As noted above, high surfactant concentrations significantly reduce γ and promote, in the absence of a magnetic field, spontaneous emulsification. This is evidenced by the microdroplets streaming off the base of the drop under the influence of gravity. The shape of the stream is highly dependent on pH (Figure 5a). At low pH, the stream bows upward as the microdroplets leave the drop and falls straight downward at high pH. This difference arises from the difference in the size of the microdroplets (as determined by light scattering) (Figure 5c; Figure S8, Supporting Information). Although the density of microdroplets is close to the density of water (1 g cm^{-3}) and, therefore, greater than that of the surrounding medium (0.867 g cm^{-3}), Brownian forces and convection (driven by small temperature gradients) become comparable to gravitational force and influence the shape of the stream.

An optical image of the microdroplets suspended in the oil phase is shown in Figure S9 (Supporting Information). Except for large droplets that sediment due to gravity (Figure S10, Supporting Information), the microdroplets are stable for at least 1 month without coalescence or loss of their magnetization. After this time, the microdroplets shrink to half their original size (Figure 5c).

3. Conclusion

In conclusion, assemblies of paramagnetic NPSs at the oil/water interface were brought into an oversaturated using an external dc magnetic field. Upon rapid removal of the field, the stored free energy is released through an explosive emulsification, a dynamical interfacial instability where an explosive ejection of a plume of ferromagnetic microdroplets from the interface occurs. The potential energy of the parent drop and ejection velocities of the microdroplets were tunable by changing the pH, surfactant concentration, and rate of removal of the permanent magnet from the drop. These findings uncover an efficient energy storage and release process, that has potential applications for remotely controlled soft microrobots, taking advantage of the ferromagnetic nature of the microdroplets. The controllable mass transfer during the explosive emulsification also endows more possibilities to realize controllable and intermittent cargo delivery, chemical shuttling in compartmentalized micro-reaction systems, and liquid external field sensors.

4. Experimental Section

Preparation of Paramagnetic Nanoparticle Surfactants at the Interface: The negatively charged carboxylic acid-functionalized iron oxide nanoparticles (Fe_3O_4-CO_2H) (Ocean NanoTech) with the diameter of ≈30 nm were superparamagnetic nanoparticles with excellent colloidal stability. One monolayer of oleic acid and one monolayer of amphiphilic polymer, totaling ≈4 nm, surrounded the ≈22 nm-sized magnetic core. They are prepared by thermos-decomposition method and each nanoparticle was a single crystal with a structure of magnetite. The Fe_3O_4-CO_2H nanoparticles were dispersed in deionized water to form the aqueous dispersion that was injected into the oil phase by the syringe to form a pendant liquid droplet.

The ω-(diethylene triamine)-terminated polystyrene (PS-triNH_2, M_w = 1200 g mol^{-1}) (Polymer Source) was dissolved in toluene to interact with Fe_3O_4-CO_2H nanoparticles (1 mg mL^{-1}), forming the magnetic NPSs at the interface. The polydispersity index (PDI) for the PS-triNH_2 (1–9 mg mL^{-1}) was 1.25, and the functionality was 98%. All nanoparticle dispersions were used without further purification and diluted to the required concentration using deionized water. The pH of the aqueous dispersions was adjusted using NaOH or HCl (1.0 M).

Interfacial Tension Measurement: A tensiometer (Krüss DSA30) was used to measure γ between water and toluene via the pendant drop method. The time dependence of γ was recorded after the aqueous droplet had been injected into the oil phase. The volume of the aqueous droplet was ≈5 µL, and the measurement time was up to 3000 s. A homemade Helmholtz coil was used to magnetize the magnetic NPSs in a uniform magnetic field up to 16 kA m^{-1}. The droplet volume remained constant in the presence of the magnetic field, indicating that the heat generated by the coil and its effect on the assembly were negligible. A NdFeB magnet was also used to magnetize the magnetic NPSs (≈175 kA m^{-1}), and 2D simulation of the magnetic field surrounding the magnet is shown in Figure S11 (Supporting Information) (COMSOL Multiphysics).

Optical Observation of the Interfacial Behavior: A digital camera on a tensiometer was used to visualize the macroscopic behavior of the magnetic NPSs at and near the interface, with the pH of aqueous phase and surfactant concentration varied. A strong bar magnet (NdFeB) was used to magnetize the droplet; the magnetic field strength and direction were the same for all measurements (Figure S11, Supporting Information). The droplets were exposed for 10 s to a magnetic field of ≈175 kA m^{-1}.

Microscopic Characterization of the Microdroplets: The micromorphology of the microdroplets was characterized by polarized optical microscopy (ZEISS Imager.A2). The diameter of the microdroplet suspended in toluene was detected by means of dynamic light scattering (Malvern Zetasizer Nano Series ZS90), and the microdroplet dispersions were prepared by spontaneously forming microdroplets at the interface of the hanging aqueous droplet in the surrounding oil phase for 3 h. The upper layer of the microdroplet dispersion was used to measure the microdroplet size without additional procedures.

Controllable Retraction Rate of the Magnet: A homebuilt stepping motor was used to control the speed of retraction of a NdFeB magnet that was attached to a translation stage. The motor speed was varied up to 1000 rpm equivalent to a velocity of 3–24.2 mm s^{-1}. The magnet was mechanically fixed to the stage to ensure the same magnetic field strength and direction for all measurements (Figure S11, Supporting Information).

Statistical Analysis: All reported experiments in this study were reproduced in triplicate to confirm data consistency. The results were expressed as mean ± standard deviation (SD). Python, ImageJ, COMSOL Multiphysics and OriginPro software were used to analyze, visualize, and plot all data.

Supporting Information

Supporting Information is available from the Wiley Online Library or from the author.

Acknowledgements

The experiments were supported by the U.S. Department of Energy, Office of Science, Office of Basic Energy Sciences, Materials Sciences and Engineering Division under Contract No. DE-AC02-05-CH11231 within the Adaptive Interfacial Assemblies Towards Structuring Liquids program (KCTR16). The authors also acknowledge the support of the Beijing Advanced Innovation Center for Soft Matter Science and Engineering at the Beijing University of Chemical Technology. R.S. acknowledges support from the National Science Foundation (NSF), Division of Materials Research (DMR) under grant no. 2203933. Work at the Molecular Foundry was supported by the Director, Office of Science, Office of Basic Energy Sciences, Division of Materials Sciences and Engineering, of the U.S. Department of Energy under Contract No. DE-AC02-05CH11231.

Conflict of Interest

The authors declare no conflict of interest.

Data Availability Statement

The data that support the findings of this study are available from the corresponding author upon reasonable request.

Keywords

explosive emulsification, magnetic field, magnetic nanoparticle surfactants, overpacked interfacial assemblies

Received: November 28, 2022
Revised: January 27, 2023
Published online:

[1] a) Z. Zhang, Y. Jiang, C. Huang, Y. Chai, E. Goldfine, F. Liu, W. Feng, J. Forth, T. E. Williams, P. D. Ashby, T. P. Russell, B. A. Helms, *Sci. Adv.* **2018**, *4*, eaap8045; b) A. Saini, K. Theis-Brohl, A. Koutsioubas, K. L. Krycka, J. A. Borchers, M. Wolff, *Langmuir* **2021**, *37*, 4064; c) G. Singh, H. Chan, T. Udayabhaskararao, E. Gelman, D. Peddis, A. Baskin, G. Leitus, P. Kral, R. Klajn, *Faraday Discuss.* **2015**, *181*, 403; d) F. Martinez-Pedrero, *Adv. Colloid Interface Sci.* **2020**, *284*, 102233; e) X. Liu, N. Kent, A. Ceballos, R. Streubel, Y. Jiang, Y. Chai, P. Y. Kim, J. Forth, F. Hellman, S. Shi, D. Wang, B. A. Helms, P. D. Ashby, P. Fischer, T. P. Russell, *Science* **2019**, *365*, 264; f) M. Cui, T. Emrick, T. P. Russell, *Science* **2013**, *25*, 460; g) X. Liu, S. Shi, Y. Li, J. Forth, D. Wang, T. P. Russell, *Angew. Chem.* **2017**, *129*, 12768; h) X. Wu, Q. Yuan, S. Liu, S. Shi, T. P. Russell, D. Wang, *ACS Macro Lett.* **2019**, *8*, 512.

[2] a) Y. Kim, G. A. Parada, S. Liu, X. Zhao, *Sci. Robot.* **2019**, 4; b) N. Bira, P. Dhagat, J. R. Davidson, *Front. Robot. AI* **2020**, *7*, 588391.

[3] a) J. Ge, H. Lee, L. He, J. Kim, Z. Lu, H. Kim, J. Goebl, S. Kwon, Y. Yin, *J. Am. Chem. Soc.* **2009**, *131*, 15687; b) J. Ge, Y. Yin, *Angew. Chem.* **2011**, *50*, 1492; c) M. Wang, L. He, Y. Yin, *Mater. Today* **2013**, *16*, 110.

[4] Y. Hu, L. He, Y. Yin, *Small* **2012**, *8*, 3795.

[5] a) J. Hasnain, Y. Jiang, H. Hou, J. Yan, L. Athanasopoulou, J. Forth, P. D. Ashby, B. A. Helms, T. P. Russell, P. L. Geissler, *J. Chem. Phys.* **2020**, *153*, 224705; b) R. Granek, R. C. Ball, M. E. Cates, *J. Phys. II* **1993**, *3*, 829; c) J. Zhu, R. C. Hayward, *Angew. Chem.* **2008**, *120*, 2143; d) S. Guttman, Z. Sapir, M. Schultz, A. V. Butenko, B. M. Ocko, M. Deutsch, E. Sloutskin, *Proc. Natl. Acad. Sci. USA* **2016**, *113*, 493; e) J. Zhu, R. C. Hayward, *J. Am. Chem. Soc.* **2008**, *130*, 7496; f) K. H. Ku, J. M. Shin, D. Klinger, S. G. Jang, R. C. Hayward, C. J. Hawker, B. J. Kim, *ACS Nano* **2016**, *10*, 5243.

[6] a) C. V. Sternling, L. E. Scriven, *AIChE J.* **1959**, *5*, 514; b) T. Okazawa, J. Bron, *J. Colloid Interface Sci.* **1979**, *69*, 86; c) L. M. Prince, *J. Colloid Interface Sci.* **1967**, *23*, 165.

[7] a) D. Cholakova, Z. Vinarov, S. Tcholakova, N. D. Denkov, *Curr. Opin. Colloid Interface Sci.* **2022**, *59*, 101576; b) G. J. Hirasaki, C. A. Miller, O. G. Raney, M. K. Poindexter, D. T. Nguyen, J. Hera, *Energy Fuels* **2010**, *25*, 555; c) K. J. Ruschak, C. A. Miller, *Ind. Eng. Chem. Fundam.* **1972**, *11*, 534; d) C. A. Miller, *Colloids Surf.* **1988**, *29*, 89; e) A. Bozeya, A. Al-Bawab, S. E. Friberg, C. A. Miller, *J. Dispers. Sci. Technol.* **2013**, *34*, 1429.

[8] a) N. Shahidzadeh, D. Bonn, J. Meunier, *Europhys. Lett.* **1997**, *40*, 459; b) N. Shahidzadeh, D. Bonn, J. Meunier, M. Nabavi, M. Airiau, M. Morvan, *Langmuir* **2000**, *16*, 9703.

[9] S. Aslan, A. Firoozabadi, *Langmuir* **2014**, *30*, 3658.

[10] a) K. Roger, U. Olsson, M. Zackrisson-Oskolkova, P. Lindner, B. Cabane, *Langmuir* **2011**, *27*, 10447; b) L. Wang, X. Q. Guan, C. C. Zheng, N. Wang, H. S. Lu, Z. Y. Huang, *Langmuir* **2020**, *36*, 10082; c) Y. H. Liu, E. L. Carter, G. V. Gordon, Q. J. Feng, S. E. Friberg, *Colloids Surf., A* **2012**, *399*, 25.

[11] H. Xie, M. Sun, X. Fan, Z. Lin, W. Chen, L. Wang, L. Dong, Q. He, *Sci. Robot.* **2019**, *4*, eaav8006.

[12] a) K. G. Marinova, R. G. Alargova, N. D. Denkov, O. D. Velev, D. N. Petsev, I. B. Ivanov, R. P. Borwankar, *Langmuir* **1996**, *12*, 2045; b) S. Pullanchery, S. Kulik, B. Rehl, A. Hassanali, S. Roke, *Science* **2021**, *374*, 1366.

[13] a) C. Huang, J. Forth, W. Wang, K. Hong, G. S. Smith, B. A. Helms, T. P. Russell, *Nat. Nanotechnol.* **2017**, *12*, 1060; b) H. Hou, J. Li, X. Li, J. Forth, J. Yin, X. Jiang, B. A. Helms, T. P. Russell, *Angew. Chem.* **2019**, *58*, 10142; c) X. Wu, R. Streubel, X. Liu, P. Y. Kim, Y. Chai, Q. Hu, D. Wang, P. Fischer, T. P. Russell, *Proc. Natl. Acad. Sci. USA* **2021**, *118*, e2017355118; d) S. Shi, X. Liu, Y. Li, X. Wu, D. Wang, J. Forth, T. P. Russell, *Adv. Mater.* **2018**, *30*, 1705800; e) J. Forth, X. Liu, J. Hasnain, A. Toor, K. Miszta, S. Shi, P. L. Geissler, T. Emrick, B. A. Helms, T. P. Russell, *Adv. Mater.* **2018**, *30*, 1707603; f) C. Huang, Y. Chai, Y. Jiang, J. Forth, P. D. Ashby, M. M. L. Arras, K. Hong, G. S. Smith, P. Yin, T. P. Russell, *Nano Lett.* **2018**, *18*, 2525.

[14] D. Guo, Y. Song, *Chemistry* **2018**, *24*, 16196.

[15] R. M. Erb, H. S. Son, B. Samanta, V. M. Rotello, B. B. Yellen, *Nature* **2009**, *457*, 999.

[16] S. R. de Groot, P. Mazur, in *Non-Equilibrium Thermodynamics*, Dover Publications, NY, USA **1984**.

[17] a) V. L. Kolev, K. D. Danov, P. A. Kralchevsky, G. Broze, A. Mehreteab, *Langmuir* **2002**, *18*, 9106; b) A. J. Prosser, E. I. Franses, *Colloids Surf., A* **2001**, *178*, 1.

[18] a) C. C. S. Pedroso, V. R. Mann, K. Zuberbühler, M.-F. Bohn, J. Yu, V. Altoe, C. S. Craik, B. E. Cohen, *ACS Nano* **2021**, *15*, 18374; b) B. Tian, A. Fernandez-Bravo, H. Najafiaghdam, N. A. Torquato, M. V. P. Altoe, A. Teitelboim, C. A. Tajon, Y. Tian, N. J. Borys, E. S. Barnard, M. Anwar, E. M. Chan, P. J. Schuck, B. E. Cohen, *Nat. Commun.* **2018**, *9*, 3082.

[19] A. R. N. Bastos, C. D. S. Brites, P. A. Rojas-Gutierrez, C. DeWolf, R. A. S. Ferreira, J. A. Capobianco, L. D. Carlos, *Adv. Funct. Mater.* **2019**, *29*, 1905474.

[20] R. Streubel, X. Liu, X. Wu, T. P. Russell, *Materials* **2020**, *13*, 2712.